Supplemental Material

Tunable magnetic textures in spin valves: From spintronics to Majorana bound states

Tong Zhou[1,*], Narayan Mohanta[2], Jong E. Han[1], Alex Matos-Abiague[2], and Igor Žutić [1]

[1]Department of Physics, University at Buffalo, State University of New York, Buffalo, NY 14260, USA

[2]Department of Physics and Astronomy, Wayne State University, Detroit, MI 48201, USA

*Address correspondence to: tzhou8@buffalo.edu

Supplemental figures:

1. Fig. S1: Oscillations of the zero energy modes splitting in longer effective topological wires with 5, 6, 7 and 9-ON MNP array.
2. Fig. S2: The calculated dispersion, probability and charge densities for MBS in 3-ON MNP array with the inclusion of spin-orbit coupling due to bulk inversion asymmetry.
3. Fig. S3: The calculated probability and charge densities for MBS coming from the subbands in 3-ON MNP array.

Extensively studied platforms for Majorana bound states (MBS), which rely on proximity-induced superconductivity in epitaxially-defined one-dimensional (1D) semiconductor nanowires (NWs) and uniform applied magnetic field, **B** [1,2], share some similar properties with our proposal in the main text where reconfigurable effective topological wires are implemented through the interplay between superconducting and magnetic proximity effects in a two dimensional electron gas (2DEG). These similarities can be already seen from the well-known topological condition for the gap closing in an infinitely long proximitized NWs, $E_{\text{Zeeman}} = (\mu^2 + \Delta^2)^{1/2}$ [1,2] as well as from the MBS formation at the ends of physical or effective wires, respectively. Tunable magnetic textures implemented in an array of magnetic nanopillars (MNPs) yield inhomogeneous effective **B**-fields and a resulting approximate generalized topological condition [Eqs. (2) and (3), main text]. For a homogeneous **B**-field, this generalized topological condition in a 2DEG reduces to the previous topological condition for 1D NWs.

However, given that we study magnetic textures with resulting fringing fields that are often ignored, but play a crucial role in forming effective topological wires in the neighboring 2DEG, we use this Supplemental Material (SM) to elucidate possible differences in the MBS formation and control, as compared to the well-known 1D NW counterparts. We recall that in our platform, in addition to generating Zeeman splitting and particle confinement, these fringing fields overcome the need for complex network of physical wires to implement braiding, as well as result in synthetic spin-orbit coupling (SOC) in the 2DEG. Within this scheme, the MBS manipulation relies on commercially available spin transfer torque (STT)-controlled magnetic textures whereby magnetization configuration in each MNP can be electrically controlled (see Fig. 1, main text).

In this SM, Fig. S1 shows the low-energy spectrum as function of the chemical potential for larger size system (5, 6, 7, 9 MNPs), where the oscillations of the zero energy states splitting are strongly suppressed with the increased number of MNPs. Given that the fringing fields already yield sufficient synthetic SOC, in Fig. S2 we also explore the influence of the Dresselhaus SOC, inherent to the III-V semiconductors [3-5]. Such intrinsic SOC has only a very small influence on the MBS formation, which in our case is dominated by synthetic SOC. Fig. S3 shows the MBS with multiple subbands. The calculated results are all obtained by accurate micromagnetic modeling of the fringing fields using a finite-element method in COMSOL [6] as an input to the Bogoliubov-de Gennes (BdG) equations, as described in the main text. Specifically, BdG are discretized using a forth order finite-difference method and verified for the convergence of their solution by refining the computational grid. Specifically, the discretized lattice spacing units are taken as 20 nm for both x and y direction in our calculations, giving 51×21, 71×21, 81×21, 91×21, 111×21, and 171×21 grid sizes for 3, 5, 6, 7, 9, and 15 MNP array, respectively. The calculations based on finer grids with the lattice spacing unit of 10 nm show the results are convergent.

[1] R. M. Lutchyn, J. D. Sau, and S. Das Sarma, Phys. Rev. Lett. **105**, 077001 (2010).
[2] Y. Oreg, G. Refael, and F. von Oppen, Phys. Rev. Lett. **105**, 177002 (2010).
[3] G. L. Fatin, A. Matos-Abiague, B. Scharf, and I. Žutić, Phys. Rev. Lett. **117**, 077002 (2016
[4] J. Fabian, A. Matos-Abiague, C. Ertler, P. Stano, and I. Žutić, Acta Phys. Slov. 57, 565 (2007).
[5] I. Žutić, J. Fabian, and S. Das Sarma, Rev. Mod. Phys. 76, 323 (2004).
[6] COMSOL Multiphysics software, http://comsol.com/.

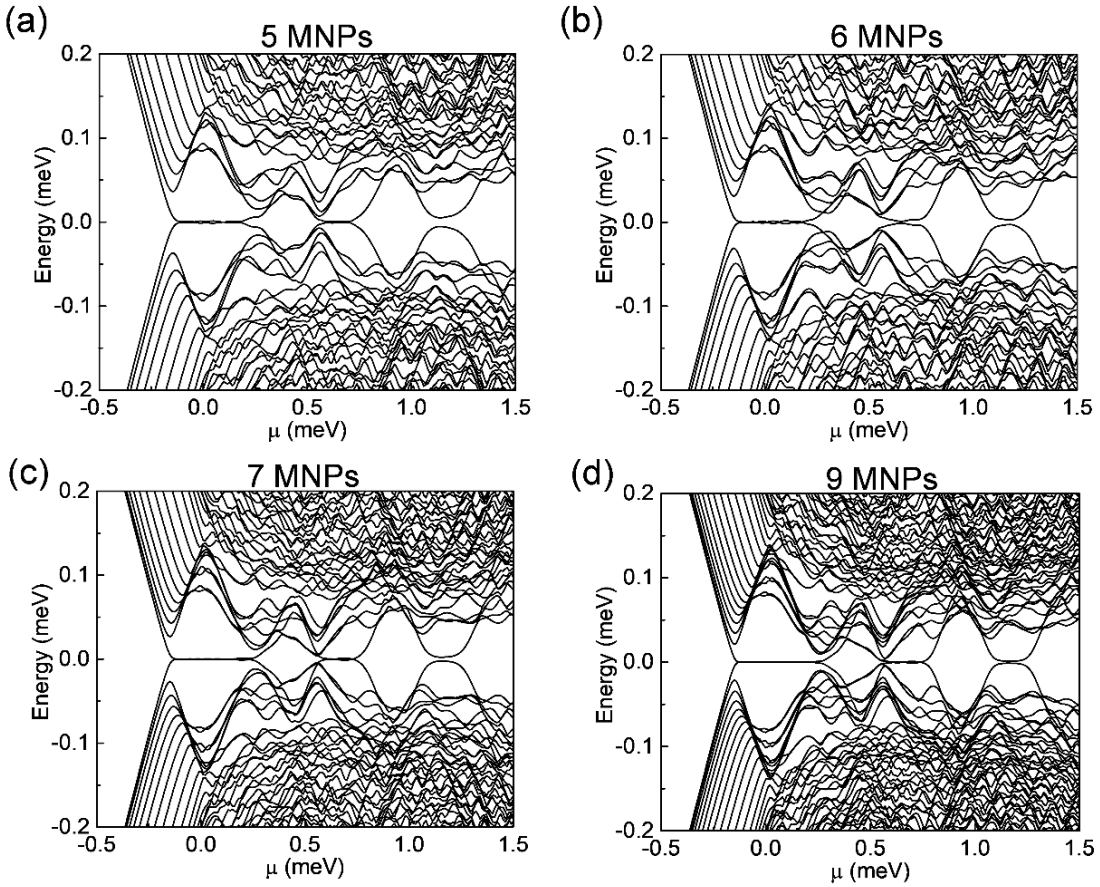

Fig. S1 (a) – (d) Low-energy spectrum as a function of the chemical potential, μ, for a system in Fig. 1, but with 5, 6, 7 and 9-ON MNP arrays, respectively. The parameters are taken from Fig. 2.

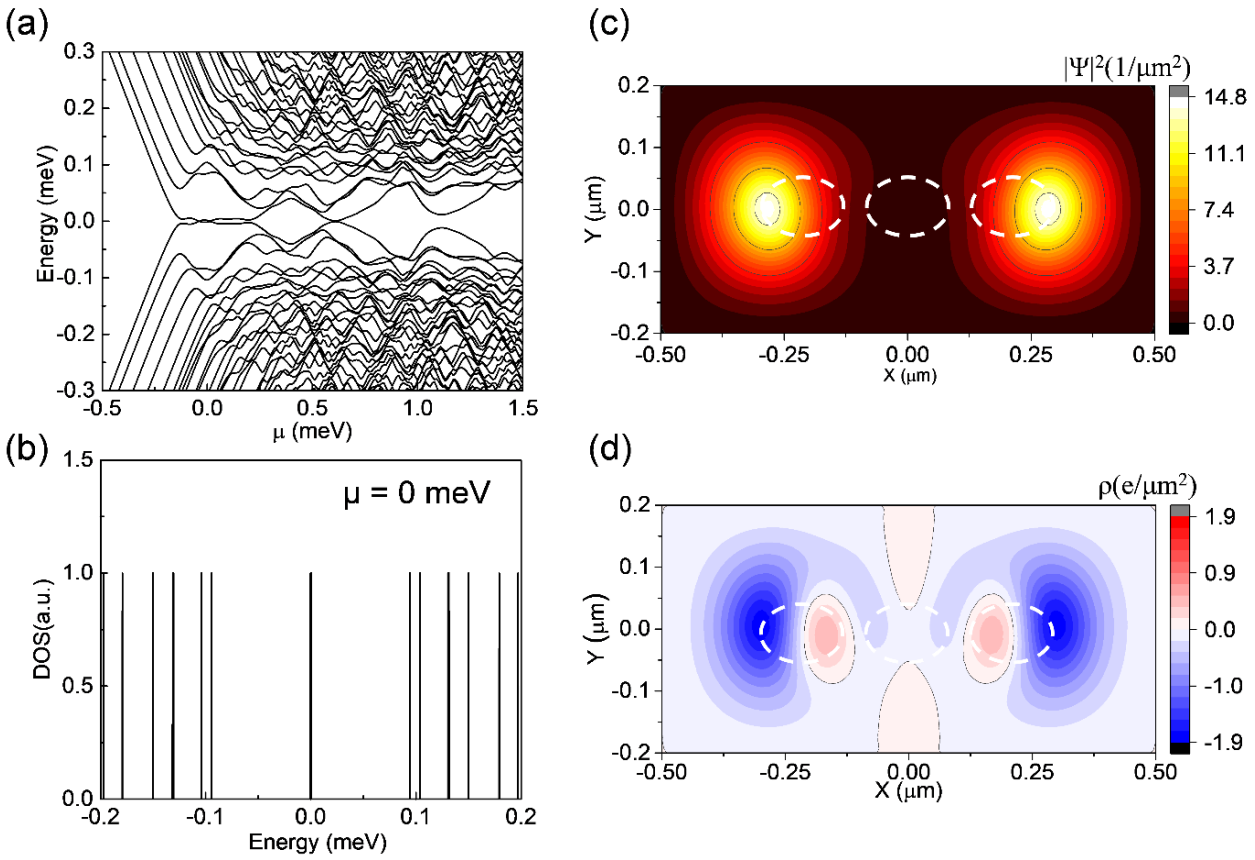

Fig. S2 (a) Low-energy spectrum as a function of the chemical potential, μ, for a system in Fig.1 with 3-ON MNP array with the inclusion of spin-orbit coupling from the bulk inversion asymmetry, written for the (110) plane as $\frac{\gamma}{\hbar} p_x \sigma_y$, where γ = 40 meVÅ is used [3-5]. (b) The density of states from (a). (c) and (d) The probability density and charge density for the lowest energy states with μ = 0. The black lines in (c) indicate the contours with the values in the color bars, and in (d) the zero-contour values. Dashed lines in (c) and (d) denote the MNP array. The parameters are taken from Fig. 2.

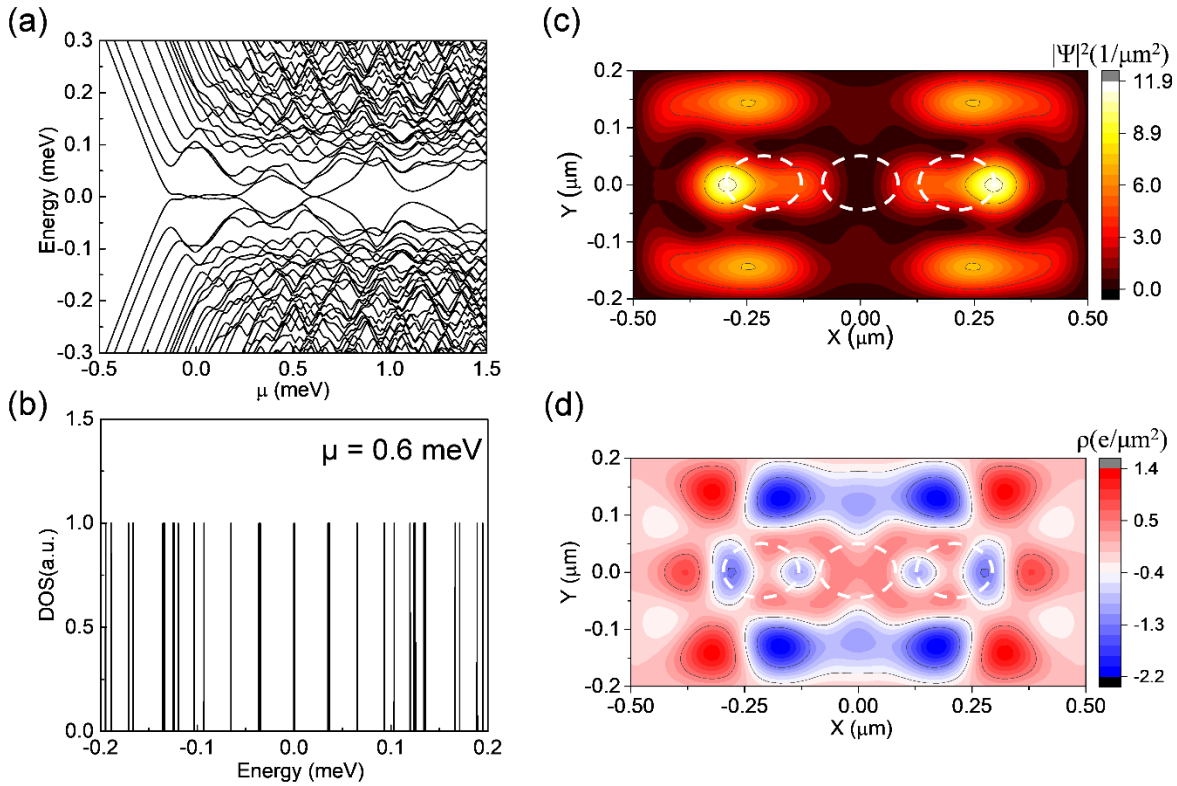

Fig. S3 (a) Low-energy spectrum as a function of the chemical potential, μ, for a system in Fig.1 with 3-ON MNP array. (b) The density of states from (a). (c) and (d) The probability density and charge density for the lowest energy states with μ = 0.6 meV. The black lines in (c) and (d) show the contours with the values in the color bars. Dashed lines in (c) and (d) denote the MNP array. The parameters are taken from Fig. 2.